Int. J. Nano Dimens., 12 (4): 355-368, Autumn 2021

ORIGINAL ARTICLE

Fabrication of PCL-PEG-PCL nanocarrier for Co-loading of Docetaxel/Quercetin and assessment of its effect on growth inhibition of human liver cancer (Hep-G2) cell line

Pejman Hakemi[1], Arezoo Ghadi[1,*], Soleiman Mahjoub[2,3], Ebrahim Zabihi[2,4], Hamed Tashakkorian[2,4]

[1]Department of Chemical Engineering, Ayatollah Amoli Branch, Islamic Azad University, Amol, Iran, Iran
[2]Cellular and Molecular Biology Research Center, Health Research Institute, Babol University of Medical Sciences, Babol, Iran
[3]Department of Clinical Biochemistry, School of Medicine, Babol University of Medical Sciences, Babol, Iran
[4]Department of Pharmacology & Toxicology, School of Medicine, Babol University of Medical Sciences, Babol, Iran

Received 02 February 2021, revised 22 May 2021, accepted 12 June 2021, available online 20 June 2021

Abstract

Nanoscale co-delivery systems are advanced examples of combination therapies that can provide better therapeutic performance. Here, we tried to improve the solubility, bioavailability, synergistic, and potentiation properties of docetaxel (DTX) using co-loading of DTX and quercetin (Qu) into PCL-PEG-PCL-based nanocarrier. To this end, PCL-PEG-PCL copolymer synthesized, then, DTX and DTX/Qu loaded into this nanocarrier, separately, by the nanoprecipitation-modified method. Physicochemical and biological properties of nanocarriers were assessed on human liver cancer (Hep-G2) and normal fibroblast cell lines, then, results were compared with free-DTX, free-Qu, and free-DTX/Qu groups. Based on the results, particles morphologically possessed a quasi-spherical shape with an average size of less than 200nm. Moreover, DTX/Qu-coloaded nanocarrier was led to further inhibition of Hep-G2 cells and lower inhibition of FNF cell viability, in a lower concentration (IC50: 29.35 µg/ml) than DTX-loaded nanocarrier (IC50: 36.73 µg/ml), free-DTX (IC50: 49.81 µg/ml), and free-DTX/Qu (IC50: 37.16 µg/ml). It could be due to the mixing of Qu and DTX that leads to an increase in the potentiation of DTX. The results also showed the release mechanism of Qu and DTX can be respectively diffusion (Fickian model) and a combination of dissolution and copolymer degradation (non-Fickian model). This was led to the higher inhibition of Hep-G2 at lower concentration of drug and higher antioxidant activity of DTX/Qu-co-loaded nanocarrier than other groups, at lower inhibition of FNF cell growth. Accordingly, the synthesized nanocarriers showed a more impact on the inhibition of cancer cells compared to normal cells, due to the synergistic effect and the created potentiation.

Keywords: *Co-delivery System; Copolymer; Docetaxel; Potentiation Effect; Quercetin; Synergistic Effect.*

How to cite this article

Hakemi P, Ghadi A, Mahjoub S, Zabihi E, Tashakkorian H. Fabrication of PCL-PEG-PCL nanocarrier for Co-loading of Docetaxel/Quercetin and assessment of its effect on growth inhibition of human liver cancer (Hep-G2) cell line. Int. J. Nano Dimens., 2021; 12(4): 355-368.

INTRODUCTION

The balance between cell division and its death is an important factor in the health and life of living beings. When this balance is upset, and the rate of cell growth/proliferation is uncontrollably greater than cell death, cancer is created. In this field, the cancers of lung, breast, liver, ovarian, prostate, and colorectal are known as the deadliest cancers that kill many patients each year. In the meantime, surgery, radiotherapy, chemotherapy, and hormone therapy are methods that are used,

* Corresponding Author Email: *arezoo.ghadi@gmail.com*

individually or in combination with each other, at different stages of the progression of cancer [1]. However, numerous side effects of these methods or low response rates of chemotherapy drugs and their low solubility/bioavailability, etc. are considered as challenges for clinical applications [2-7]. In this field, docetaxel (DTX) is a potent anti-mitotic chemotherapy drug that is commonly used for the treatment of metastatic cancers such as liver, lung, head and neck cancers, etc.[1, 3, 6]. However, the large polycyclic structure of DTX limits the solubility and clinical applications of this drug[6]. Thus, DTX commercially contains high concentrations of polysorbate 80 (Tween-80) and ethanol which leads to side effects such as shortness of breath, hepatotoxicity, inflammatory and neurological reactions, cumulative fluid retention, etc. [1, 5-7]. Moreover, neutropenia, leukopenia, edema, diarrhea, and fatigue have been observed after DTX administration due to the non-specific distribution of the drug in the body [1, 8, 9]. Notably, although DTX effectively suppresses the target, however, it is ineffective in overcoming survival signals activated in response to treatment and leads to multidrug resistance (MDR) [10, 11]. Therefore, the prevention of multidrug resistance and signaling pathways (such as Akt) can lead to the development of a new therapeutic strategy to overcome multidrug resistance and metastasis. Nanoscale drug delivery systems (NDDSs) are one of the more important methods in this field.

Indeed, single loading of DTX on synthesized nanocarriers can increase the solubility and bioavailability of DTX and reduce potential side effects. In contrast, the co-loading of this drug with a suitable pharmacological agent can, in addition to solubility and bioavailability, also increase the response rate of DTX. The reports have shown that concomitant use of anti-cancer drugs and quercetin (Qu) can increase the bioavailability of the drug, synergistic and potentiation effects[2, 4]. Indeed, the Qu is an AKT inhibitor and a potent flavonoid and possesses high antioxidant activity and can prevent tumor metastasis. Qu also suppresses extracellular signal-regulated kinase signaling pathways. However, the simultaneous administration of several drugs with different physicochemical properties is a major challenge due to the drug composition's variable pharmacokinetics, that Nanoscale drug delivery systems can solve this problem. However, NDDSs possess many disadvantages, such as the slow or incomplete release of the drug(s) into the cell, nanoparticle instability, and early release, etc. [12]. Hence, the various nanocarriers have been developed as targeted drug delivery systems. In this regard, polymeric micelles have several advantages compared to other nano-systems, including easy preparation, effective and relatively high loading of the drug, controlled and stable release of the drug in target tissue [12-14]. Notably, the polymer micelles structure is as core/shell and is usually formed by self-assembly of blocks of amphiphilic copolymers [1, 13, 15].

Nowadays, copolymers of two and three amphiphilic blocks containing hydrophilic and hydrophobic strings have gotten attention in the medical and biology industry, especially for hydrophobic drugs delivery [16, 17].

Several synthetic polymers such as poly (ethylene glycol) (PEG), polyglycolide (PGA), polylactide (PLA), and poly (ε-caprolactone) (PCL) are used in drug delivery systems due to predictable degradation kinetics and ease of formulation [18].

In this field, PCL is used more often in medical applications due to a relatively long-degradation time and low-cost than other polymers [19, 20]. Moreover, PEG as a polymer of nontoxic, biocompatible, non-immunogenic, and hydrophilic [18, 21], can control the pharmacokinetic behavior of the drug and degradation kinetics and improve biodegradability. This polymer can also provide an appropriate approach to overcome the problems of the use of PCL such as accumulation in vivo, low compatibility with targeted tissues, and low biodegradability that can lead to a non-controlled release of drugs or drug instability in the micro-environment of the polymer [17, 22-25]. Hence, it seems that binary and ternary copolymers containing these polymers, as an amphiphilic carrier can form micelles in an aqueous environment due to hydrophobic interaction in lipophilic parts.

Therefore, this study aimed to fabricate the PCL-PEG-PCL triblock copolymer-based nanocarrier to co-encapsulate of DTX and Qu that can lead to an increase in synergistic/potentiation effects of DTX and drug response rates as well as a decrease in oxidative stress for normal cells. To this end, PEG6000 and PCL were selected, and after the design of copolymer, DTX, and Qu were loaded into the nanocarrier. Afterward, the physicochemical properties of micelles along with

biological properties of nanocarriers co-loaded with both drugs and single-DTX were evaluated on the human liver (Hep-G) cancer cell lines

EXPERIMENTAL

Materials

Quercetin (Qu), docetaxel (DTX), Poly(ethylene glycol) (PEG, Mn: 6000 Da), poly(ε-caprolactone) (PCL, purity > 98%), phosphate-buffered saline tablets (PBS), tin(II) 2-ethyl hexanoate [stannous octoate: Sn(Oct)2], dichloromethane (DCM), diethyl ether, and tetrazolium salt 3-(4, 5-dimethylthiazol-2-yl)-2,5-diphenyltetrazolium bromide (MTT) were purchased from Sigma-Aldrich (UK). Acetone, acetonitrile, and methanol (HPLC grade) were purchased from MERK (Germany). The human liver cancer cell line (Hep-G2, NCBI Code: C158) were obtained from the national cell bank of Iran (NCBI) (Pasteur Institute, Iran). The foreskin normal fibroblast cell line (FNF) was purchased from Babol University of Medical Sciences. Moreover, Foetal bovine serum (FBS), and RPMI-1640 medium (Roswell Park Memorial Institute) were also obtained from Gibco (USA).

Preparation of PCL-PEG–PCL copolymer

The PCL-PEG–PCL triblock copolymer was prepared by ring-opening polymerization of PEG and ε-caprolactone (ε-CL) in the presence of $Sn(Oct)_2$ as the catalyst [26, 27]. To this end, PEG (4 g) and ε-CL (8 g) were added to 0.01 mmol $Sn(Oct)_2$ and heated under a nitrogen atmosphere for 10 min (130°C). Then, the solution was mixed at 150°C, under the stirring condition for 6 h, and then cooled at 25°C. Afterward, this mixture dissolved in DCM for 20 min. Finally, cold diethyl ether was added to the mentioned mixture, and the precipitated copolymer was dried under vacuum (25 °C, 48 h).

Characterization of triblock copolymer

The chemical structure of the PCL-PEG-PCL copolymer was studied by FTIR-spectrum analysis (Fourier Transform Infrared Spectroscopy, Model-ALPHA, Bruker, Germany) and spectra were acquired from 400-4000 cm-1 with 4 cm-1 resolution. Moreover, the average molecular weight of the mentioned copolymer was also determined by gel permeation chromatography (GPC) (Knauer, Berlin, Germany) which is set with the differential refractometer detector and an ultras Tyra gel column (4.6×30 mm) (Waters, Milford, USA, model HR 4E). Notably, tetrahydrofuran (THF) was used as the mobile phase [flow-rate: 1 ml/min, the injection volume: 50 µl of stock solutions (0.1-0.5 w/v %)] and mono-disperse polystyrene as standard in the range of 1500-35,500 Da (Varian Palo Alto, CA).

Co-loading of drugs into nano-carriers

The Qu/DTX-co-loaded nano-carriers were prepared by a modified nanoprecipitation method [28]. Briefly, 16 mg of PCL-PEG-PCL copolymers, 2 mg of DTX, and 2 mg of Qu were dissolved in 2 mL of acetone and stirred in a dark environment at 25 °C (6 h). The organic phase was added into 25 mL of water via a syringe (G-22), under consistent mixing, and was stirred at 25°C, to evaporate the solvent and form micelles. To remove the unloaded DTX and Qu, the obtained yellowish solution was filtered by a filter membrane (0.45 µm). Finally, nano-carriers were obtained by freeze-dring at -80°C. Notably, the blank nano-carriers (without drugs) and DTX-loaded nanocarriers (with 4 mg) were prepared using the mentioned method.

The mechanism of co-loading of drugs into nanocarrier

Here, the matrix loading system with the pre-loading approach was used to load the drugs by the nanoprecipitation method (Fig. 1).

Given the structure of PCL-PEG-PCL amphiphilic copolymer (two hydrophobic blocks and a hydrophilic block), the matrix structure possesses a hydrophobic core and a hydrophilic shell which is classified as a micelle. To this end, the hydrophobic drug and amphiphilic copolymer were first dissolved in an organic solvent. Then, to form micelles, the solution was transferred to the aqueous phase under vigorous stirring. Notably, docetaxel and quercetin trapped in the hydrophobic core of synthesized micelles due to their hydrophobic nature. However, given the higher solubility of quercetin in the organic phase compared to docetaxel, it seems that a larger amount of quercetin molecules are trapped in the hydrophobic core. The assessment of encapsulation percentage can confirm the amount of loading.

Drug Loading and Encapsulation Efficiency

The HPLC device was used to determine the percentage of drug loading (DL%) and encapsulation efficiency (EE%). Initially, the

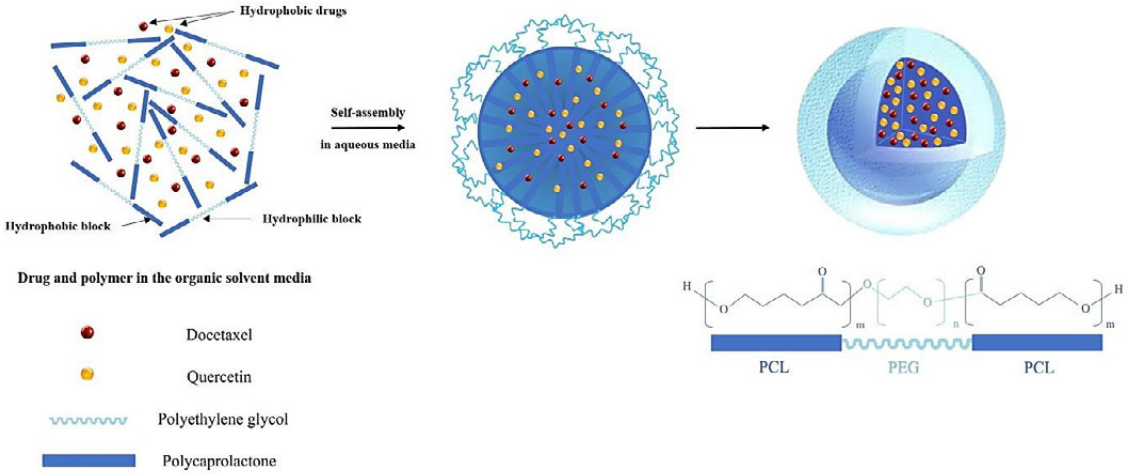

Fig. 1. The mechanism of co-loading of DTX/Qu into PCL-PEG-PCL nanocarrier.

absorbance-concentration standard curve of docetaxel and quercetin was plotted using three different concentrations (3 repetitions). Then, the lyophilized powder was dissolved in 10 ml of methanol and stirred at 25°C for 1. Then 40 µl of each solution was injected into the HPLC. The drug content in the nanocarrier was determined using high-performance liquid chromatography (HPLC). Notably, the HPLC analyses were performed by a system equipped with a C-18 reversed-phase column (150×4.6 mm, 5 µm, C-18; KNAUER Technologies). The DTX detection wavelength and the elution rate were 227 nm and 1.0 ml/min, respectively, as well as the mixture of acetonitrile and water (50:50 v/v), was applied as the mobile phase. The Qu was also detected at 374 nm using methanol and 5% (w/v) acetic acid as the mobile phase at the volume ratio of 70:30 (v/v) [elution rate: 1 mL/min, T: 25°C]. Finally, the EE (%) and DL (%) were obtained by equations 1 and 2.

$$\%EE = \frac{\text{weight of drug in micelles}}{\text{weight of initial drug}} \times 100 \quad (1)$$

$$\%DL = \frac{Weight\ of\ drug\ in\ micelles}{Weight\ of\ micelles} \times 100 \quad (2)$$

Study of size, PDI, and zeta potential

The size, zeta potential, and polydispersity index (PDI) of all samples were measured by dynamic light scattering (DLS) (Malvern Instruments, Worcestershire, UK, model Nano ZS).

Morphology of nanocarriers

The morphology of these samples (with and without drug) was also studied using a scanning electron microscope (SEM, XL30 ESEM, Philips, Germany), To this end, 2 µl of the blank nanocarrier, DTX-loaded nanocarrier, and Qu/DTX-co-loaded nanocarrier solutions was separately placed onto a substrate (1 cm2) and then air-dried. The average size of nanocarriers was determined by Clemex vision software 3.5 by choosing 25 locations on the surfaces randomly.

Study of drug release

In vitro drug release test was carried out to assess the release behavior of the drug-co-loaded/loaded NCs. Briefly, 10 mg of dried drug-loaded nanocarriers were dispersed in PBS [4 ml, pH: 7.4 and 5.5] and this suspension was dialyzed by a dialysis sac (Mw: 12000 Da) and incubated at 37°C, while immersed in PBS. At different time intervals, 3 ml of PBS solution was withdrawn and replaced by 3 ml fresh PBS. Finally, the concentrations of DTX and Qu in the dialysate were determined by HPLC (tests were performed in triplicate).

Drug release kinetics

To determine the kinetic of drug release from the NC, release data were studied by the kinetic model of Korsmeyer-Peppas, at pH 7.4 and 5.5. Korsmeyer-Peppas kinetic provides a simple and semi-empirical model where the drug release is exponentially related to the fractional release of the drug (Eq. 3) [29].

$$\left(\frac{M_t}{M_\infty}\right) = K.t^n \quad (3)$$

M_∞ : the amount of drug at the equilibrium state
Mi: the amount of drug released over time t
K: the considered the release velocity constant
n: the exponent of release in the function of time t

Notably, the n value and the type of release behavior can imply the Fickian model (Case I: 0.45 ≤ n ≤ 0.5, the drug release corresponds diffusion) or Non-Fickian models (Case II: n = 1, the drug release rate relates to zero-order kinetic, and the driving mechanism of the drug is related to the swelling or relaxation of polymeric chains, Anomalous Case: 0.5 < n < 1, the drug release corresponds diffusion and swelling, and Super Case II: n > 1, the tension and breaking of the polymer during the sorption process) [30-32].

Cell Culture

In vitro experiment was performed on the Hep-G2 as cancer cell line, and FNF as normal cell line to assess the biological efficiency of the drug-co-loaded nanocarrier. To this end, the cells were seeded at a density of 3×104 cells per well (as optimum cell concentration), into a culture medium contains RPMI-1640, 10% FBS, and 100 U/mL penicillin/100 µg/ml streptomycin, and then the plates were incubated at 37°C (humidified atmosphere, 5 % CO2) for 48 and 72 h.

Cytotoxicity (MTT) assay

Followed by, an MTT assay was performed to study the effect of the drug-loaded/co-loaded nanocarriers and free drugs on Hep-G2 and FNF cell lines at concentrations of 25, 50, 100, and 200 µg/ml. In Brief, the medium of each well was removed and replaced by 100 µl of fresh medium and 20 µl of MTT solution. After incubation for 4 h, the MTT medium was removed, then 200 µl of DMSO was added to each well, and the absorbance of samples was obtained at a wavelength of 570 nm. Finally, the cell viability (%) was calculated by equation 4. The control group was defined as cells without treatment and the viability of the mentioned cells in this group was considered as 100%. IC50 (half-maximal inhibitory concentration) values using MTT assay were also determined on a Log-scale.

$$\text{Cell viability}\,(\%) = \frac{\text{OD}_{treated\ cells}}{\text{OD}_{control\ cells}} \times 100 \quad (4)$$

OD: Optical density is proportional to the mass in the cell suspension.

Measurement of total antioxidant capacity

To evaluate the antioxidant activity of samples, the FRAP (Ferric Reducing Antioxidant Power) method was used, which is based on the reduction of ferric pyridyl triazine complex to ferrous pyridyl triazine at low pH in the presence of antioxidants.

To this end, the FRAP reagent components include 10 mmol/L TPTZ (2, 4, 6-Tripyridyl-S-triazine) in 40 mmol/L HCL, 20 mmol $FeCl_3.6H_2O$, 0.3 M acetate buffer, 3.1 g of sodium acetate mixed with acetic acid (16 ml), and then volume reach 1 liter. The final pH was adjusted to 3.6 and The FRAP reagent was kept at 4 °C and in colored containers to protect the light. Notably, the different concentrations of ferrous sulfate (125, 250, 500, and 1000 µmol/ml of FeSO4.7H2O) as standard solutions were prepared, and the standard curve was plotted.

Afterward, to perform the FRAP test, 1.5 ml of the prepared FRAP reagent (acetate buffer, TPTZ reagent, and ferric chloride solution with the ratio of 10:1:1, respectively) was added to each tube. All tubes were incubated at 37°C for 5 min. 50 µl of the sample, standard, and blank (distilled water) was added to the tubes and then mixed gently. The tubes were then incubated again at 37 °C and finally, the absorbance rate of the product and optical absorption of each sample along with and standard solution were determined using a spectrophotometer (Jenway 6505, UK) at 593 nm and the results were reported based on the µM [33].

Statistical analysis

All tests were carried out in triplicate. The results were expressed as mean ± standard deviation (SD) (in IBM SPSS Statistics 24 software, using the ANOVA test, P-values of <0.05 as the significance level).

RESULTS AND DISCUSSION

Physicochemical properties of triblock copolymer

FTIR spectra of PCL, PEG, PCL-PEG-PCL were shown in Fig. 2. As shown in this Figure, a strong peak at 1728 cm-1 along with several peaks at 1100-1250 cm−1 appeared in the PCL-PEG-PCL spectrum associated with the carboxylic ester (C=O) and ether (C–O) groups, respectively. Moreover, the PCL-PEG-PCL copolymer was led

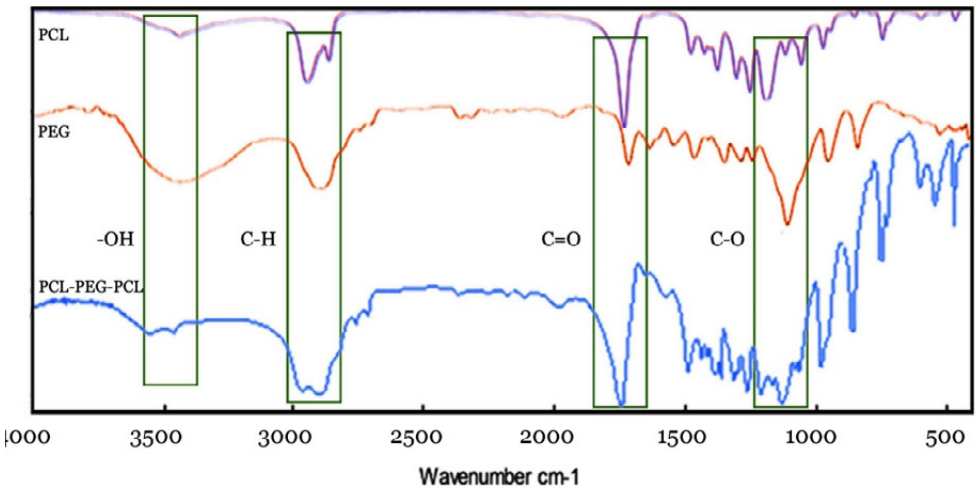

Fig. 2. FT-IR spectra of PCL, PEG, and PCL–PEG–PCL.

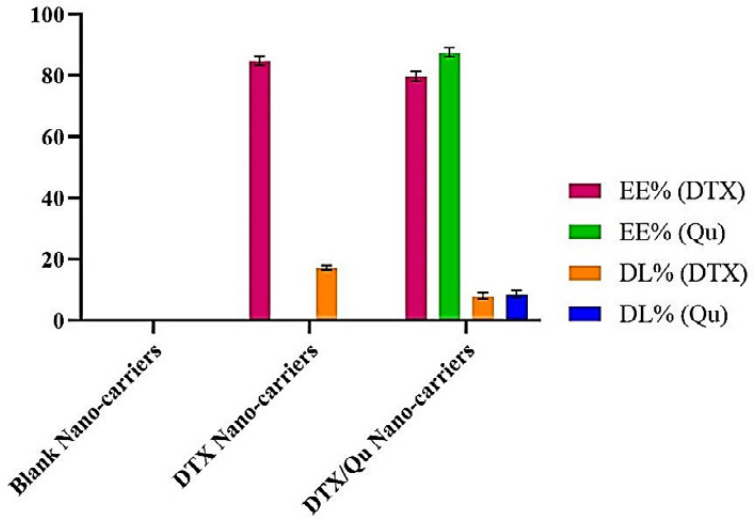

Fig. 3. The encapsulation efficiency (%) and drug loading (%) of DTX and Qu for samples containing DTX and DTX/Qu.

to a decrease in intensity of -OH peak (3439 cm-1) and shift of C-H peak (2863 and 2951 cm-1), compared with the mentioned peaks in PEG and PCL, respectively. The comparison of spectra can confirm the formation of PCL-PEG-PCL copolymer via the ring-opening polymerization of caprolactone in presence of PEG.

Moreover, the GPC analysis indicated that no transesterification/backbiting reaction has occurred during the ring-opening polymerization. So that, a single-peak was observed in the GPC-chromatogram of the PCL-PEG-PCL copolymer, which has been implied the mono-distribution of molecular weight and absence of both homopolymers of ε-CL and PEG. Based on the GPC results, Mw and Mn were determined 15188 Da and 13810 Da, respectively, as well as, polydispersity index of the polymers (PDI: Mw/Mn) was 1.09 that indicates PCL-PEG-PCL copolymer is a controlled synthetic polymer due to a value of $1.02 \leq Mw/Mn \leq 1.10$ [29, 34].

Characterization of drug-loaded nano-carriers
Determination of EE% and DL%

The percentage of encapsulation efficiency and drug loading of DTX for both samples of DTX and

DTX/Qu were 85.4±4.6 and 17.08±0.92; as well as 80.2±3.2 and 8.02±0.2, respectively. Encapsulation efficiency and loading ratio in the sample of DTX/Qu were also reported 87.8±3.3 and 8.78±0.33, respectively. As observed in Fig. 3, the co-loading of drugs was led to a decrease in EE% and DL% of DTX that can be due to repulsive forces between particles and interaction between two drugs.

Assessment of size, zeta potential, and PDI

The average diameter, zeta potential, and PDI of synthesized nano-carriers were measured by DLS.

As shown in Fig. 4a, the average diameter and zeta potential of blank nanocarrier, DTX-loaded, and DTX/Qu-coloaded nanocarriers were reported to be 115.1 nm, -11.8 mV; 122.8 nm, -10.49 mV; and 161.9 nm, -9.2 mV, respectively. The increase in the zeta potential for DTX/Qu-coloaded nanocarrier can be explained by oppositely charged ions related to the co-loading of the drug which leads to a long residence time in the body. Notably, nanoparticles with a zeta potential of between -10 and +10 mV are considered almost neutral [35]. The results demonstrated that the PDI of the mentioned nanocarriers were 0.369, 0.357, and 0.256, respectively.

Based on the studies, the drug-loaded nanocarrier with average diameters less than 200 nm along with PDI of about 0.35 (required PDI for pharmaceutical nanoparticles) can be easily transferred to target sites via the circulatory

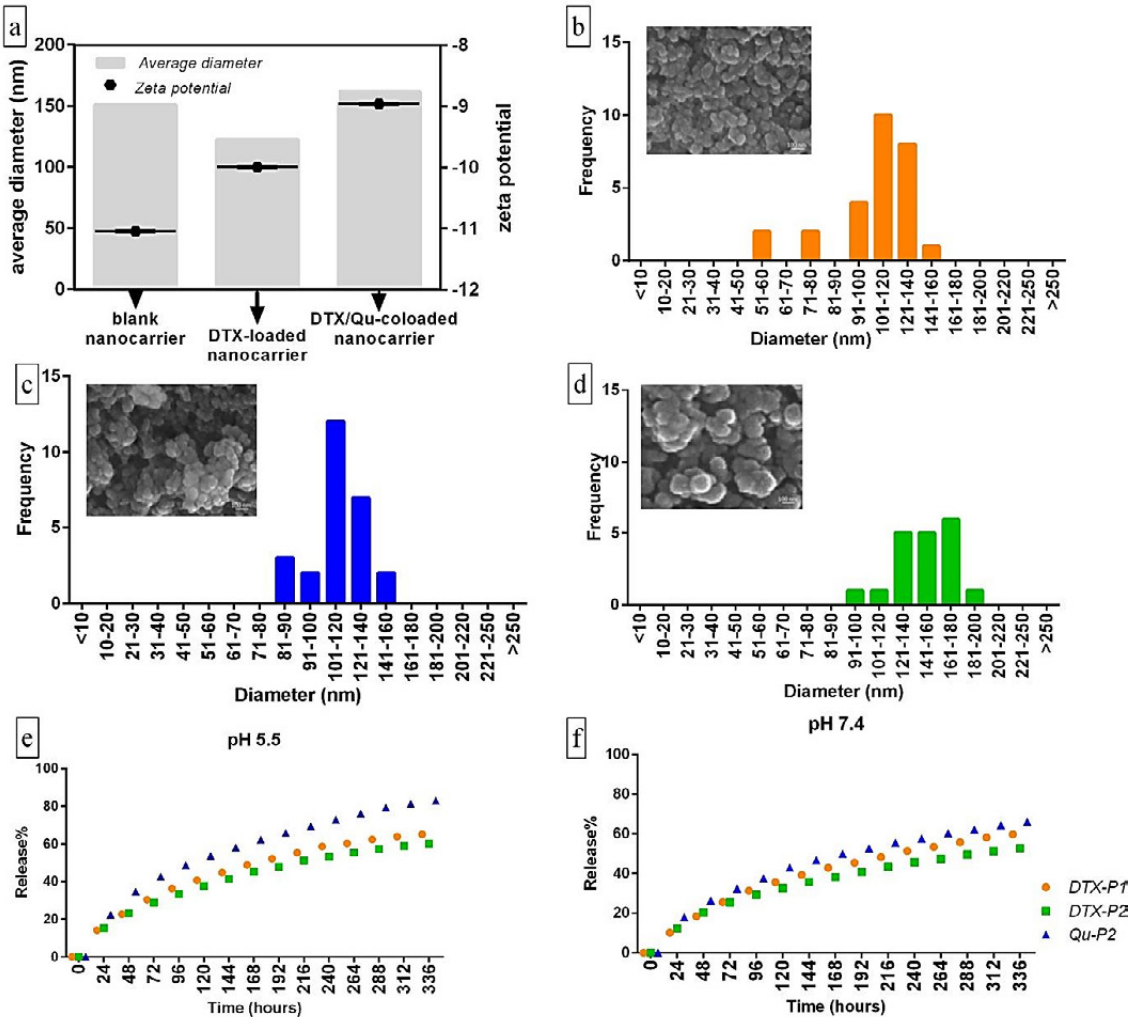

Fig. 4. The average diameter and zeta potential (a), along with SEM images for P0 (b), P1 (c), and P2 (d). Drug release from Drugs-loaded nanocarrier at pH of 5.5 (e) and 7.4 (f).

system [36-40]. Hence, it seems that DTX/Qu-coloaded nanocarriers can be suitable for drug delivery applications.

Morphology of nanocarriers

The surface morphology and the diameter distribution of nanocarriers have been shown by scanning electron microscopy (SEM) (Fig. 4 b-d).

The SEM images demonstrate that the particles possess a quasi-spherical shape. Moreover, the related histogram of nanocarriers indicates that the average size of the nanocarriers varied from 115 to 162nm, so that average size for P0, P1, and P2 was respectively determined 109.62 nm ± 23.48, 115.72 nm ± 16.95, and 149.61 nm ± 24.46. The comparison of the sizes of the nanocarriers showed that the size of particles is significantly dependent on drug loading into the nanocarrier. Notably, the average size of nanocarriers obtained by the DLS method was greater than those by SEM, because the DLS technique measures the hydrodynamic diameter (HD) of particles in suspension.

Study of drug release

The in vitro drug release from DTX-loaded nanocarrier (P1) and DTX/Qu-co-loaded nanocarrier (P2) in PBS solutions (pHs 5.5 and 7.4) were investigated by the dialysis method (Fig. 4e and f).

The release of both drugs from the P1 and P2 nanocarriers at pH 5.5 occurred in two parts include explosive release along with a slow and stable release. Based on the results, in the first 120 h, the release of DTX from the P1 and P2 was 41% and 38%, respectively. While, in the next 216 h, only 22% to 24% of DTX was released from the nanocarriers. Moreover, the Qu release from the P2 was 54%, in the first 120 h, and then, this value increased to ~70% during 216 h (Fig. 4e). The 7.32% decrease of DTX release from P2 compared to P1 could be due to co-loading of DTX and Qu, and interaction into the copolymer matrix, as well as the more inclination of Qu for the faster release.

Likewise, the release pattern of both drugs from the P1 and P2 at pH 7.4, similar to pH 5.5, began with a rapid upward trend, and then led to a sustained release. The based on the results, DTX release from the P1 nanocarrier was ~35%, in the first 120 h. While at the same time, the P2 nanocarrier was led to the release of ~33% of the DTX and 43% of the Qu. Afterward, the upward trend in drug release from both P1 and P2 nanocarriers continued, so that the release of 60% and 53% for DTX respectively in P1 and P2, and 66% for Qu was obtained in the final 336 h (Fig. 4f). Hence, it is clear that the synthesized nanocarrier with PCL-PEG-PCL copolymer possesses a stable release in 336 h and pH-sensitive property that can be applied to target pH outside the cancer cell membrane.

Such that, the decrease of pH values leads to faster swelling of nanocarrier shell and more dissolution in the environment, resulting in the rapid release of encapsulated DTX and Qu. Furthermore, the faster release of the Qu can be explained by the lower molecular weight and the improvement in the solubility of this drug compared to DTX.

Drug release kinetic

The drug release kinetic from the synthesized nanocarriers was studied by the Korsmeyer-Peppas model. Given that the Korsmeyer-Peppas equation applies to polymer systems, it is expected that the mentioned equation will be most consistent with the synthesized nano-carriers.

The fitting of the released data from both nanocarriers along with the constants of K and the values of n have shown in Fig. 5a-d and Table 1. Notably, 60% of the released drug at the specified time was used in this equation. To this end, the Korsmeyer-Peppas equation was first linearized, then, a fraction of the data obtained from drug release (60%) was fitted into the plot. The sum of the squares of the error (R2) obtained from drug release data for both nanocarriers indicated that the Korsmeyer-Peppas model possesses good concordance with the release data in both pHs 7.4 and 5.5 (Table 1).

Given the n values (exponent of drug release) in the Korsmeyer-Peppas equation, it was found that the mechanism of DTX release encapsulated into both nanocarriers corresponds to the non-Fickian model (Fig. 5a and b) [41, 42]. Although, it cannot be precisely stated that this model shows the exact mechanism of drug release, but drug have been released from the synthesized nano-carriers is affected by multiple and complex conditions. In contrast, the mechanism of Qu release corresponded to the Fickian model and diffusion mechanism that can be due to the lower molecular weight of Qu (302.24 Da) compared to DTX (861.93 Da).

Notably, the decrease of pH indicated a higher

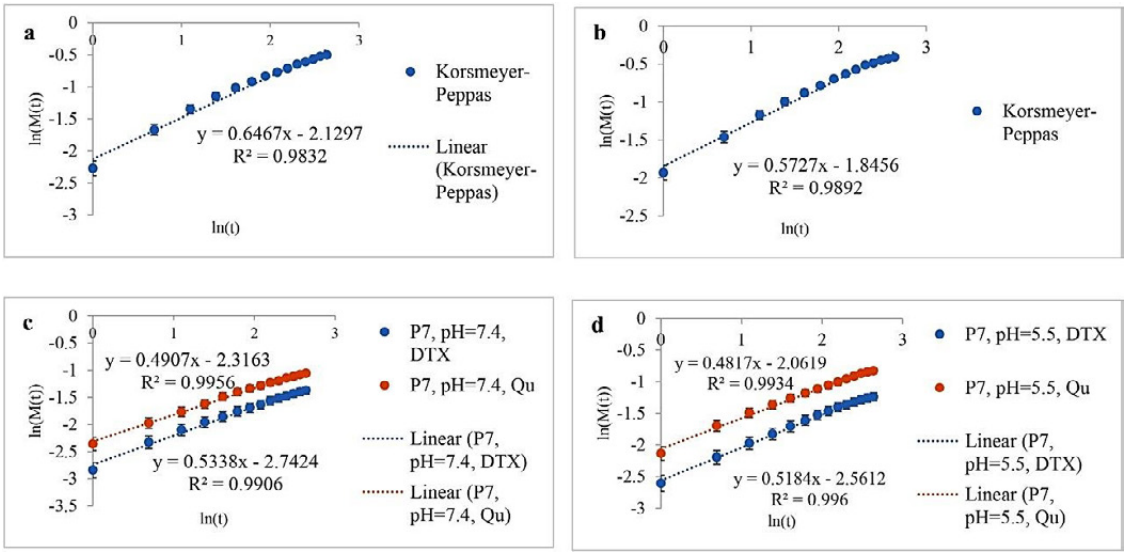

Fig. 5. The drug release kinetic from the synthesized nanocarriers by the Korsmeyer-Peppas model, for DTX-loaded nanocarrier (a: pH 7.4 and b: 5.5) and DTX/Qu-co-loaded nanocarrier (c: pH 7.4 and d: 5.5).

Table 1. The values of K, n, and R2 of the Korsmeyer-Peppas model.

pH	nano-Carriers	$K_{(DTX)}$	$n_{(DTX)}$	$R^2_{(DTX)}$	$K_{(Qu)}$	$n_{(Qu)}$	$R^2_{(Qu)}$	Equation $(\frac{M_t}{M_\infty}) = K.t^n$	
								DTX	Qu
7.4	P4	0.1188	0.6467	0.9832	NA	NA	NA	y=0.6467x- 2.1297	NA
5.5	P4	0.1579	0.5727	0.9892	NA	NA	NA	y=0.5727x-1.8456	NA
7.4	P7	0.0644	0.5338	0.9906	0.0986	0.4907	0.9956	y=0.5338x- 2.7424	y=0.4907x- 2.3163
5.5	P7	0.0772	0.5184	0.996	0.1272	0.4817	0.9934	y=0.5184x- 2.5612	y=0.4817x- 2.0619

rate in Qu release via diffusion that implies pH-sensitivity of nanocarrier network (Fig. 5a and d). The comparison of DTX release in both pHs of 7.4 and 5.5 can confirm this point, such that, the decrease in pH was led to a decrease in n value and its approach to the Fickian model and the diffusion process.

Here, given the type of copolymer and the nanocarriers synthesis method, it seems that the release mechanism to be a two-step process. Initially, the drugs close to the surface of the nanocarrier or adsorbed to the surface with weak bonds, and drugs with a lower molecular weight under ambient conditions (temperature, pH, salt, molecular interactions of the environment, and the surface of the nanocarrier) are released. In the next stage, the polymer is gradually degraded due to ambient conditions such as pH-sensitivity, the ratio of hydrophobicity and hydrophilicity, the interactions between drugs and polymers, etc. and it leads to the release of the drug [43, 44].

Given the DTX release profile and low solubility of this drug in water, the mechanism of its release may be the combination of dissolution and copolymer degradation. Moreover, the increase in the amount of Qu release compared to DTX can be due to the higher solubility and lower molecular weight of Qu.

Cell viability assay

The in vitro cytotoxicity of the synthesized nanocarriers and the free drugs were evaluated by the MTT method. To this end, the cancerous cells of Hep-G2, and fibroblast normal cells (FNF) were exposed to different concentrations of free-DTX, free-Qu, free-DTX/Qu, empty nanocarrier (P0), DTX-loaded nanocarrier (P1), and DTX/Qu-coloaded nanocarrier (P2) for 48 and 72 h. The viability percentage of Hep-G2 and fibroblast cells has shown in Fig. 6.

As shown in this Figure, the lowest percentage of Hep-G2 cells viability for all studied groups at 48 h and 72 h was related to the concentration of 200µg/ml (Fig. 6a and b). The results of this study on the P1 and P2 also showed, although the mentioned concentration was led to a decrease in the growth of FNF cells, however more cells of FNF survive than cancerous cells of Hep-G2

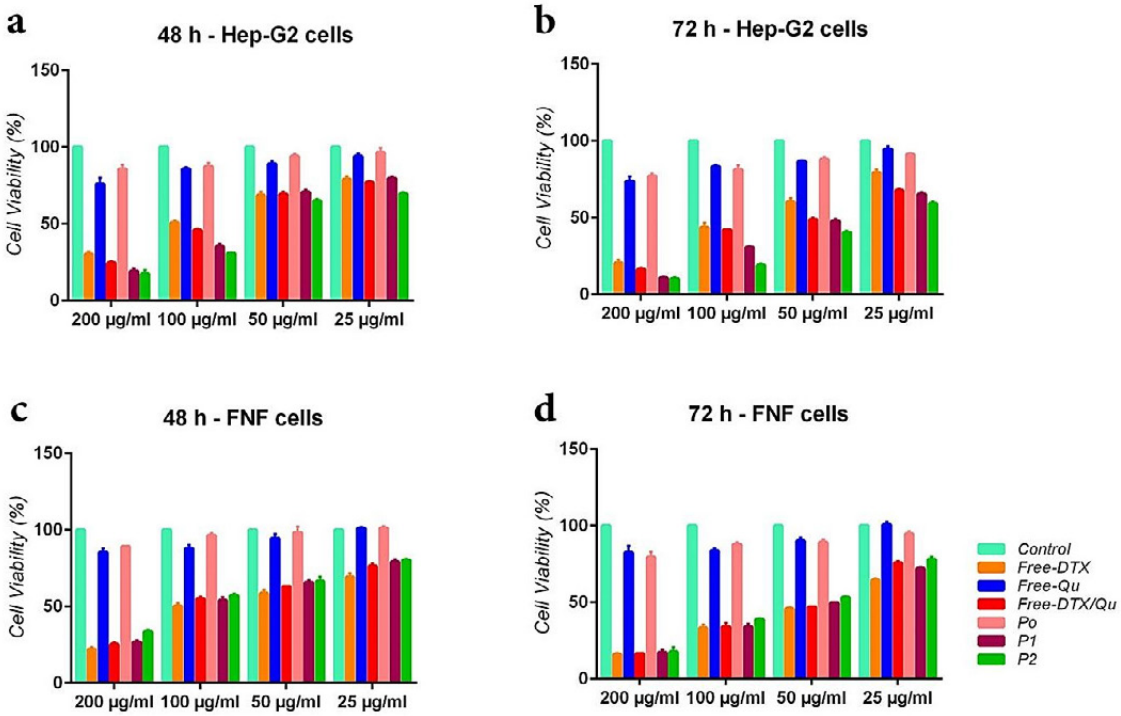

Fig. 6. The viability of Hep-G2 and FNF cells at four concentrations for free-drugs and synthesized nanocarriers loaded/co-loaded with drugs, during 48h (a and c) and 72 h (b and d).

Table 2. The IC50 value of free-DTX, free-DTX/Qu, P1 (DTX-loaded nanocarriers), and P2 (DTX/Qu-loaded nanocarriers) on both cell lines of cancerous and normal.

Groups	IC_{50}			
	Hep-G2 cell	R^2	FNF cell	R^2
Free-DTX	49.81	0.9752	32.29	0.9870
Free-DTX.Qu	37.16	0.9653	39.51	0.9884
P1	36.73	0.9843	38.30	0.9903
P2	29.35	0.9926	44.66	0.9831

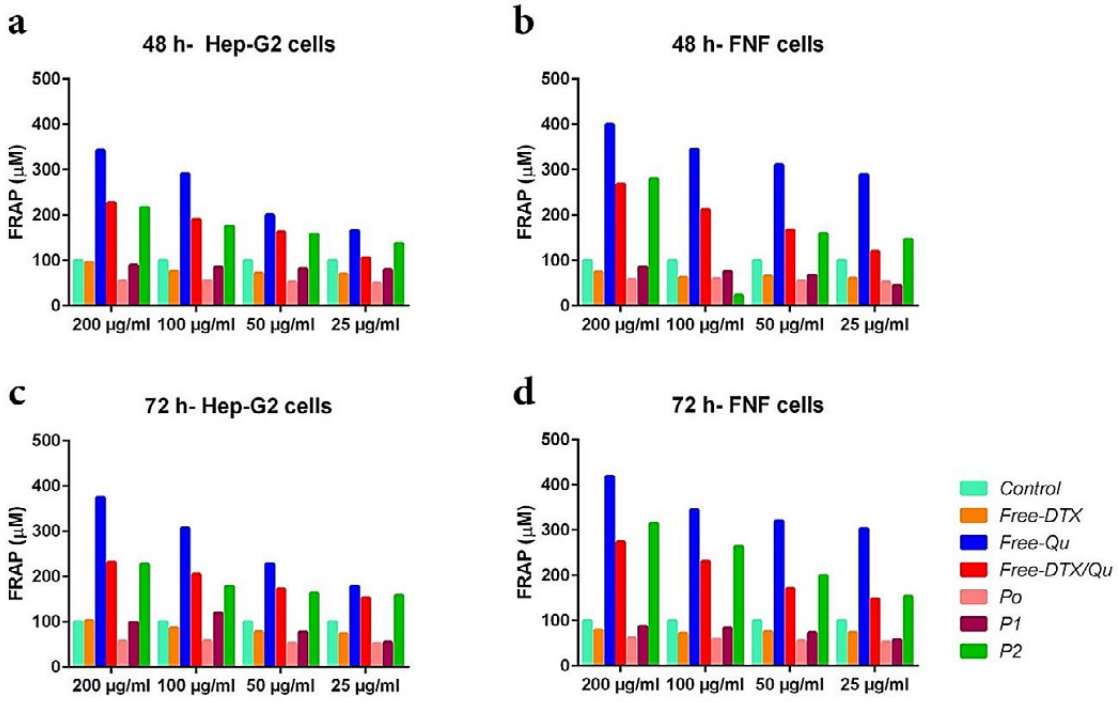

Fig. 7. Total antioxidant capacity of Hep-G2 and FNF cells treated with the synthesized nanocarriers compared to free-DTX, free-Qu, and free-DTX/Qu at 48 h (a and b) and 72 h (c and d).

(Fig. 6a and d). It can be due to the antioxidant properties of Qu that lead to a decrease in cytotoxicity of DTX drug in normal cells. The cell viability% of FNF treated with free-Qu, for all concentrations and at both time of 48 h and 72 h, can confirm the positive effect of Qu in this field (more than 80%). Moreover, cell viability% of more than 85% for P0 means that nanocarrier is ineffective for the cells. It is also found that the lowest viability% of Hep-G2 cells, at all four in all concentrations and both time of 48 h and 72 h, has related to P2 than P1, free-DTX, and free-DTX/Qu. It could be due to the slow release of the drug and it's kinetic, as well as drug availability over a longer period of time.

Furthermore, the results of IC50 indicated that P2, in a lower concentration than P1, free-DTX, and free-DTX/Qu, was led to further inhibition of Hep-G2 cells and lower inhibition of FNF cell viability (Table. 2). It can be due to the co-encapsulation of DTX and Qu that resulted in high potentiation of DTX to inhibit Hep-G2 proliferation [4, 45-48]. The comparison of IC50 between P1 and P2 as well as between free-DTX and free-DTX/Qu of the Hep-G2 cells confirms the effect of this potentiation. Notably, the free-DTX-Qu mix and co-loading of these drugs into nanocarrier possessed lower toxicity on the FNF (as normal cells) compared to free-DTX and P1, which could be due to antioxidant properties of Qu.

Total antioxidant capacity

In vitro, the total antioxidant capacity of the synthesized nano-carriers and the free-drug was evaluated, by the FRAP method (Fig. 7a-d).

The P2 nanocarrier showed higher antioxidant activity at both cell lines compared to P1 and free-DTX. This can confirm the MTT and IC50 results for higher inhibition of Hep-G2 growth and lower inhibition of cell viability of FNF cells by P2. It also observed that antioxidant activity of free-DTX/Qu on the Hep-G2 cells was higher than P2, at all concentrations studied and both times of 48 h (Fig. 7a and b) and 72 h (Fig. 7c and d), which can be related to free-drug, the potentiation of DTX mixed with Qu, and easier/better access to Qu. However, the opposite result was observed for these two groups on the normal cell line of FNF. It could be due to the presence of free-DTX and its negative effect on the FNF growth.

It was also found that free-Qu possesses higher antioxidant activity compared to other groups at both cell lines tested. Indeed, the Qu is a powerful antioxidant [49, 50], hence, samples containing Qu show more antioxidant activity than other groups.

Notably, the decrease in the concentration of all studied groups led to a decrease in the antioxidant activity of nanoparticles. It shows that the total antioxidant activity is dependent on the concentration of Qu, and concentration change leads to the change of FRAP index [51].

The comparison of results also indicated that the antioxidant activity depends on time, so that, with the increase of time, the FRAP index has increased. This can help to decrease the toxicity of DTX on the normal cells and enhance FNF cells proliferation, as well as higher inhibition of Hep-G2 cells due to potentiation of DTX with Qu in P2 and free-DTX/Qu.

CONCLUSION

This study aimed at DTX/Qu- coloaded nanocarriers to promote the therapeutic efficacy of DTX, decrease its side effects. The results demonstrate that the synthesized PCL-PEG-PCL copolymer possesses an average size of less than 200 nm and pH-sensitivity. Moreover, biologically this copolymer as an empty nanocarrier (P0) was non-toxic and possessed biocompatibility property for normal cells. Notably, morphologically the synthesized nanocarrier was possessed quasi-spherical structures and dimensions and its encapsulation% was observed more than 80%. Based on the results, DTX/Qu-coloaded nanocarrier was led to further inhibition of Hep-G2 cells (as cancerous cells) and lower inhibition of FNF cell viability (as normal cells), in a lower concentration (IC50: 29.35 µg/ml) than DTX-loaded nanocarrier (IC50: 36.73 µg/ml), free-DTX (IC50: 49.81 µg/ml), and free-DTX/Qu (IC50: 37.16 µg/ml). It could be due to the increase in potentiation of DTX when mixed with Qu, mechanism of drugs release from nanocarrier, and antioxidant properties of Qu. Indeed, it seems that the release mechanism to be a two-step process, so that, initially the drug with a lower molecular weight (Qu) under ambient conditions and the Fickian model as the diffusion process are released. Afterward, with the degradation of the polymer due to ambient conditions such as pH-sensitivity, etc., the DTX is released based on the non-Fickian model. This mechanism of release also leads to the higher antioxidant activity of Qu in DTX/Qu-co-loaded into nanocarrier than free-DTX/Qu on the normal cell line. Given the advantages of the synthesized nanocarrier for the co-delivery system of drugs, such as the greater effectiveness of DTX, controlled release, as well as the use of lower dosage for higher inhibition of cancerous cells compared to other groups, in vivo experiments on animal models are suggested as the next step.

ACKNOWLEDGMENTS

We thank Dr. Hadi Parsian for his help in the synthesis of results.

DECLARATION OF COMPETING INTEREST

The authors declare that there are no conflicts of interest.

FORMATTING OF FUNDING SOURCES

This research did not receive any specific grant from funding agencies in the public, commercial, or not-for-profit sectors.

REFERENCES

[1] Emami J., Kazemi M., Hasanzadeh F., Minaiyan M., Mirian M., Lavasanifar A., (2020), Novel pH-triggered biocompatible polymeric micelles based on heparin–α-tocopherol conjugate for intracellular delivery of docetaxel in breast cancer. *Pharm Dev. Technol*. 25: 492-509.

[2] Alibolandi M., Abnous K., Hadizadeh F., Taghdisi S. M., Alabdollah F., Mohammadi M., Ramezani M., (2016), Dextran-poly lactide-co-glycolide polymersomes decorated with folate-antennae for targeted delivery of docetaxel to breast adenocarcinoma in vitro and in vivo. *J. Control Release*. 241: 45-56.

[3] Dadras P., Atyabi F., Irani S., Ma'mani L., Foroumadi A., Mirzaie Z. H., Dinarvand R., (2017), Formulation and evaluation of targeted nanoparticles for breast cancer theranostic system. *Eur. J. Pharm. Sci*. 97: 47-54.

[4] Li J., Zhang J., Wang Y., Liang X., Wusiman Z., Yin Y., Shen Q., (2017), Synergistic inhibition of migration and invasion of breast cancer cells by dual docetaxel/quercetin-loaded nanoparticles via Akt/MMP-9 pathway. *Int. J. Pharm*. 523: 300-309.

[5] Hu Q., Rijcken C. J., Bansal R., Hennink W. E., Storm G., Prakash J., (2015), Complete regression of breast tumor with a single dose of docetaxel-entrapped core-cross-linked polymeric micelles. *Biomaterials*. 53: 370-378.

[6] Zafar S., Akhter S., Ahmad I., Hafeez Z., Rizvi M. M. A., Jain G. K., Ahmad F. J., (2020), Improved chemotherapeutic efficacy against resistant human breast cancer cells with co-delivery of Docetaxel and Thymoquinone by Chitosan Grafted Lipid nanocapsules: Formulation optimization, in vitro and in vivo studies. *Colloids Surf. B*. 186: 110603-110607.

[7] Raza K., Thotakura N., Kumar P., Joshi M., Bhushan S., Bhatia A., Katare O. P., (2015), C60-fullerenes for delivery of docetaxel to breast cancer cells: a promising approach for enhanced efficacy and better pharmacokinetic profile. *Int. J. Pharm*. 495: 551-559.

[8] Logie J., Ganesh A. N., Aman A. M., Al-Awar R. S., Shoichet M. S., (2017), Preclinical evaluation of taxane-binding peptide-modified polymeric micelles loaded with docetaxel in an orthotopic breast cancer mouse model. *Biomaterials*. 123: 39-47.

[9] Kushwah V., Katiyar S. S., Agrawal A. K., Gupta R. C., Jain S., (2018), Co-delivery of docetaxel and gemcitabine using PEGylated self-assembled stealth nanoparticles for improved breast cancer therapy. *Nanomedicine: Nanomedicine: NBM*. 14: 1629-1641.

[10] Muthu M. S., Avinash Kulkarni S., Liu Y., Feng S. S., (2012), Development of docetaxel-loaded vitamin E TPGS micelles: formulation optimization, effects on brain cancer cells and biodistribution in rats. *Nanomed. J*. 7: 353-364.

[11] Au K. M., Min Y., Tian X., Zhang L., Perello V., Caster J. M., Wang A. Z., (2015), Improving cancer chemoradiotherapy treatment by dual controlled release of wortmannin and docetaxel in polymeric nanoparticles. *ACS Nano*. 9: 8976-8996.

[12] Asadi N., Annabi N., Mostafavi E., Anzabi M., Khalilov R., Saghfi S., Akbarzadeh A., (2018), Synthesis, characterization and in vitro evaluation of magnetic nanoparticles modified with PCL–PEG–PCL for controlled delivery of 5FU. *Artif Cells Nanomed Biotechnol*. 46: 938-945.

[13] Abasian P., Ghanavati S., Rahebi S., Nouri Khorasani S., Khalili S., (2020), Polymeric nanocarriers in targeted drug delivery systems: A review. *Polym. Adv. Technol*. 31: 2939-2954.

[14] Tiwari G., Tiwari R., Sriwastawa B., Bhati L., Pandey S., Pandey P., Bannerjee S. K., (2012), Drug delivery systems: An updated review. *Int. J. Pharm. Invest*. 2: 2-8.

[15] Moretton M. A., Bernabeu E., Grotz E., Gonzalez L., Zubillaga M., Chiappetta D. A., (2017), A glucose-targeted mixed micellar formulation outperforms Genexol in breast cancer cells. *Eur. J. Pharm. Biopharm*. 114: 305-316.

[16] Gökçe Kocabay Ö., İsmail O., (2020), Preparation and optimization of biodegradable self-assembled PCL-PEG-PCL nano-sized micelles for drug delivery systems. *Int. J. Polym. Mater*. 1-10.

[17] Kheiri Manjili H., Sharafi A., Attari E., Danafar H., (2017), Pharmacokinetics and in vitro and in vivo delivery of sulforaphane by PCL–PEG–PCL copolymeric-based micelles. *Artif. Cells Nanomed. Biotechnol*. 45: 1728-1739.

[18] Stewart S. A., Domínguez-Robles J., Donnelly R. F., Larrañeta E., (2018), Implantable polymeric drug delivery devices: Classification, manufacture, materials, and clinical applications. *Polym. J*. 10: 1379-1384.

[19] Goonoo N., Jeetah R., Bhaw-Luximon A., Jhurry D., (2015), Polydioxanone-based bio-materials for tissue engineering and drug/gene delivery applications. *Eur. J. Pharm. Biopharm*. 97: 371-391.

[20] Odom E. B., Eisenberg D. L., Fox I. K., (2017), Difficult removal of subdermal contraceptive implants: A multidisciplinary approach involving a peripheral nerve expert. *Contraception*. 96: 89-95.

[21] Song Z., Feng R., Sun M., Guo C., Gao Y., Li L., Zhai G., (2011), Curcumin-loaded PLGA-PEG-PLGA triblock copolymeric micelles: Preparation, pharmacokinetics and distribution in vivo. *J. Colloid Interf. Sci*. 354: 116-123.

[22] Manjili H. K., Malvandi H., Mousavi M. S., Attari E., Danafar H., (2018), In vitro and in vivo delivery of artemisinin loaded PCL–PEG–PCL micelles and its pharmacokinetic study. *Artif. Cells Nanomed. Biotechnol.* 46: 926-936.

[23] Feng R., Song Z., Zhai G., (2012), Preparation and in vivo pharmacokinetics of curcumin-loaded PCL-PEG-PCL triblock copolymeric nanoparticles. *Int. J. Nanomedicine*. 7: 4089-4093.

[24] Liu S., Qin S., He M., Zhou D., Qin Q., Wang H., (2020), Current applications of poly (lactic acid) composites in tissue engineering and drug delivery. *Compos. B. Eng*. 199: 108238-108243.

[25] Singh V., Tiwari M., (2010), Structure-processing-property relationship of poly (Glycolic Acid) for drug delivery systems: Synthesis and catalysis. *Int. J. Polym. Sci.*. 2010: Article ID 652719.

[26] Danafar H., Sharafi A., Kheiri Manjili H., Andalib S., (2017), Sulforaphane delivery using mPEG–PCL co-polymer nanoparticles to breast cancer cells. *Pharm. Dev. Technol*. 22: 642-651.

[27] Danafar H., (2016), Applications of copolymeric nanoparticles in drug delivery systems. *Drug Res*. 66: 506-519.

[28] Danafar H., (2017), Study of the composition of polycaprolactone/poly (ethylene glycol)/polycaprolactone copolymer and drug-to-polymer ratio on drug loading efficiency of curcumin to nanoparticles. *Jundishapur J. Nat. Pharm. Prod*. 12: e34179.

[29] Ramteke K. H., Dighe P. A., Kharat A. R., Patil S. V., (2014), Mathematical models of drug dissolution: A review. *Sch. Acad. J. Pharm*. 3: 388-396.

[30] Ritger P. L., Peppas N. A., (1987), A simple equation for description of solute release II. Fickian and anomalous release from swellable devices. *J. Control Release*. 5: 37-42.

[31] Siepmann J., Peppas N. A., (2001), Mathematical modeling of controlled drug delivery. *Adv. Drug Deliv. Rev*. 48: 139-157.

[32] Bruschi M. L., (2015), Strategies to modify the drug release from pharmaceutical systems. *Woodhead Publishing*.

[33] Benzie I. F., Strain J. J., (1996), The ferric reducing ability of plasma (FRAP) as a measure of "antioxidant power": the FRAP assay. *Anal. Biochem*. 239: 70-76.

[34] Steinman N. Y., Bentolila N. Y., Domb A. J., (2020), Effect of molecular weight on gelling and viscoelastic properties of poly (caprolactone)–b-poly (ethylene glycol)–b-poly (caprolactone) (PCL–PEG–PCL) Hydrogels. *Polym. J*..12: 2372-2378.

[35] Masarudin M. J., Cutts S. M., Evison B. J., Phillips D. R., Pigram P. J., (2015), Factors determining the stability, size distribution, and cellular accumulation of small, monodisperse chitosan nanoparticles as candidate vectors for anticancer drug delivery: Application to the passive encapsulation of [14C]-doxorubicin. *Nanotechnol. Sci. Appl*. 8: 67-72.

[36] Bahadori F., Dag A., Durmaz H., Cakir N., Onyuksel H., Tunca U., Hizal G., (2014), Synthesis and characterization of biodegradable amphiphilic star and Y-shaped block copolymers as potential carriers for vinorelbine. *Polym. J*. 6: 214-242.

[37] Hu C., Chen Z., Wu S., Han Y., Wang H., Sun H., Zhu D., (2017), Micelle or polymersome formation by PCL-PEG-PCL copolymers as drug delivery systems. *Chin. Chem. Lett*. 28: 1905-1909.

[38] Dahmoune F., Rezgui F., G'Sell C., (2016), Full factorial design optimization of anti-inflammatory drug release by PCL–PEG–PCL microspheres. *Mater. Sci. Eng. C*. 58: 412-419.

[39] Choi H. S., Liu W., Misra P., Tanaka E., Zimmer J. P., Ipe B. I., Frangioni J. V., (2007), Renal clearance of quantum dots. *Nat. Biotechnol*. 25: 1165-1170.

[40] Peer D., Karp J. M., Hong S., Farokhzad O. C., Margalit R., Langer R., (2007), Nanocarriers as an emerging platform for cancer therapy. *Nat. Nanotechnol*. 2: 751-760.

[41] Jahromi L. P., Ghazali M., Ashrafi H., Azadi A., (2020), A comparison of models for the analysis of the kinetics of drug release from PLGA-based nanoparticles. *Heliyon*. 6: e03451.

[42] Dash S., Murthy P. N., Nath L., Chowdhury P., (2010), Kinetic modeling on drug release from controlled drug delivery systems. *Acta Pol. Pharm*. 67: 217-223.

[43] Zhou W., Li C., Wang Z., Zhang W., Liu J., (2016), Factors affecting the stability of drug-loaded polymeric micelles and strategies for improvement. *J. Nanopart. Res*. 18: 1-18.

[44] Ahmad Z., Shah A., Siddiq M., Kraatz H. B., (2014), Polymeric micelles as drug delivery vehicles. *RSC Adv*. 4: 17028-17038.

[45] Altintas R., Ciftci O., Aydin M., Akpolat N., Oguz F., Beytur A., (2015), Quercetin prevents docetaxel-induced testicular damage in rats. *Andrologia*. 47: 248-256.

[46] Lu X., Yang F., Chen D., Zhao Q., Chen D., Ping H., Xing N., (2020), Quercetin reverses docetaxel resistance in prostate cancer via androgen receptor and PI3K/Akt signaling pathways. *Int. J. Biol. Sci*. 16: 1121-1127.

[47] Shitole A. A., Sharma N., Giram P., Khandwekar A., Baruah M., Garnaik B., Koratkar S., (2020), LHRH-conjugated, PEGylated, poly-lactide-co-glycolide nanocapsules for targeted delivery of combinational chemotherapeutic drugs Docetaxel and Quercetin for prostate cancer. *Mater. Sci. Eng. C*. 114: 111035-111039.

[48] Xu C., Ding Y., Ni J., Yin L., Zhou J., Yao J., (2016), Tumor-targeted docetaxel-loaded hyaluronic acid-quercetin polymeric micelles with p-gp inhibitory property for hepatic cancer therapy. *RSC Adv*. 6: 27542-27556.

[49] Gao X., Wang B., Wei X., Men K., Zheng F., Zhou Y., Wei Y., (2012), Anticancer effect and mechanism of polymer micelle-encapsulated quercetin on ovarian cancer. *Nanoscale*. 4: 7021-7030.

[50] Wu T. H., Yen F. L., Lin L. T., Tsai T. R., Lin C. C., Cham T. M., (2008), Preparation, physicochemical characterization, and antioxidant effects of quercetin nanoparticles. *Int. J. Pharm.*. 346: 160-168.

[51] Dueñas M., Surco-Laos F., González-Manzano S., González-Paramás A. M., Santos-Buelga C., (2011), Antioxidant properties of major metabolites of quercetin. *Eur. Food Res. Technol*. 232: 103-111.